Electronic structure and elasticity of two-dimensional metals of group 10: A DFT study

Journal of Physics: Conference Series **2518** (2023) 012006 doi:10.1088/1742-6596/2518/1/012006

Electronic structure and elasticity of two-dimensional metals of group 10: A DFT study

Kameyab Raza Abidi and Pekka Koskinen

NanoScience Center, Department of Physics, University of Jyväskylä, 40014 Jyväskylä, Finland.

E-mail: kameyab.r.abidi@jyu.fi

Abstract. The discovery of two-dimensional (2D) iron monolayer in graphene pores stimulated experimental and computational material scientists to investigate low-dimensional elemental metals. There have been many advances in their synthesis, stability, and properties in the last few years. Inspired by these advancements, we investigated the electronic structure and elasticity of free-standing monolayers of group 10 elemental metals, viz. Ni, Pd, and Pt. Using density-functional theory (DFT), we explored the energetic, geometric, electronic, and elastic properties of hexagonal, honeycomb, and square lattice structures of each element, in both planar and buckled forms. Among planar configurations, the order of increasing stability is honeycomb, square, and hexagonal. In buckled form, this ordering remains the same for Pt but is reversed for Ni and Pd. Upon geometrical optimization, the extent of buckling for Pt was found to be small compared to Ni and Pd. The effect of buckling on the electronic structure was further scrutinized through the projected density of states, and it was found that highly buckled configurations derive their of states from 3D bulk, which highlights the correlation between buckled configurations and 3D bulk. For Pt in buckled square and honeycomb lattices, the density of states correlates more closely to their 2D monolayers. Regarding elasticity, the in-plane elastic constants indicate that all planar and buckled square lattices are unstable.

1. Introduction

The revelation of two-dimensional (2D) iron monolayer in graphene pores [1] stimulated computational material scientists to investigate the 2D elemental metals [2–9]. Theoretical studies have suggested that several 2D metals could exist either as freestanding monolayers, buckled monolayers, or patches embedded within graphene pores. Density functional theory (DFT) studies suggested that some of the 2D metals are unexpectedly stable against bending, and their bending moduli are comparable to the bending modulus of graphene or other layered 2D materials [6]. The magnetic properties of 2D metals in different lattices were studied by Yinti Ren et al. [10] and it was found that 18 elemental 2D metals exhibit magnetism. The most preferable lattice for magnetism was found to be honeycomb, followed by hexagonal and square. For the search for energetic stability of binary alloys of 2D metals, the high-throughput DFT was used in Ref. [11]. It was identified that out of 1081 binary compounds, 41 different binary compounds are dynamically stable in a buckled honeycomb lattice structure. Motivated by this finding a systematic investigation on the dynamical stability of buckled honeycomb alloy of the noble metals (Cu, Ag, and Au) were performed [12] and it was revealed that 48 alloys of noble metals in the buckled form are dynamically stable. Alongside theoretical investigations of 2D

metals, there have been several advances in experimental research and these advancements are reported in recent review articles in a systematic manner [13–16].

2D elemental metals are still a relatively new field of research and are driven primarily by theoretical and a few experimental studies mentioned above. In this article, to understand the properties and electronic structure of elemental metals, we focused only on group 10 elemental metals. This group features elements that belong from *3d* (Ni), *4d* (Pd), and *5d* (Pt) series, and typically crystallizes in face-centered cubic (fcc) structure. In comparison to bulk systems, 2D planar and buckled metal systems are thinner, and reduced dimensionality possesses a reduced number of coordination sites for chemical bonding. This leads to differences in their mechanical, electronic, and optical properties. The buckling effect can influence the stability and strength of the chemical bonds, and it can result in a different distribution of electrons in the system, leading to differences in the electronic structures and other properties. These features make 2D planar and buckled metal systems promising candidates with tailored properties for applications in fields such as electronics, catalysis, and energy storage [17, 18]. With a low coordination number and reduced interaction between neighbouring atoms, it is reasonable to expect that the 2D systems will give rise to distinct geometric, electronic, and elastic properties from that of 3D bulk. Herein, we used the first-principles approaches using DFT to study 2D lattices (honeycomb, square, and hexagonal) of the chosen metals. All elements were considered in planar as well as in their buckled form. The cohesive energy, bond lengths, and in-plane elastic parameters were computed and compared. The electronic structure was analysed using the projected density of states (PDOS) on *s*, *p*, and *d* orbitals and compared with the 3D bulk.

2. Computational Methods

The spin-polarized density functional theory (DFT) calculations were performed using the QuantumATK [19]. The core electrons were traced by projector augmented wave (PAW) potential, and the valence electron orbitals were extended on the basis of plane waves (PW) with the energy cut-off of 800 eV [20, 21]. The non-empirical Perdew-Burke-Ernzerhof (PBE) form of the generalized gradient approximation (GGA) exchange-correlation functional was used in all calculations [22]. This choice of exchange-correlation functional is reasonable for the systems lacking empirical data and able to produce reliable energetics, electronic structure, and mechanical properties for the metals. Three different 2D systems, the honeycomb (HC), square (SQ), and hexagonal(HEX) were studied in planar as well as in buckled form (Figure 1). To obtain the self-consistent electron density, the total energy convergence criteria of 10^{-7} eV was employed. Geometry optimizations of the structures were done by using the LBFGS algorithm [23]. Optimized structures have the forces smaller than 1 meVÅ^{-1} and stresses below 0.3 meVÅ^{-3}. The k-point sampling was done using the Monkhorst-Pack method [24]. The Fermi-Dirac smearing scheme was used with a broadening of 0.05 eV.

3. Results and Discussion

3.1. Convergence Analysis:

We performed the convergence analysis to set the converged k-point and vacuum along the non-periodic direction of the 2D systems. The convergence tests were conducted on the planar systems of each elemental metal.

3.1.1. Convergence test for k-point: While performing the k-point convergence test we used the lattice parameters from the Atlas of 2D metals [6]. A vacuum of 15 Å was used along the non-periodic direction to diminish the spurious interactions between two layers of the adjacent unit cell. We calculated the total energy difference by using

$$\Delta \mathrm{E} = \mathrm{E}_{N_k \times N_k \times 1} - \mathrm{E}_{30\times 30\times 1}\,, \tag{1}$$

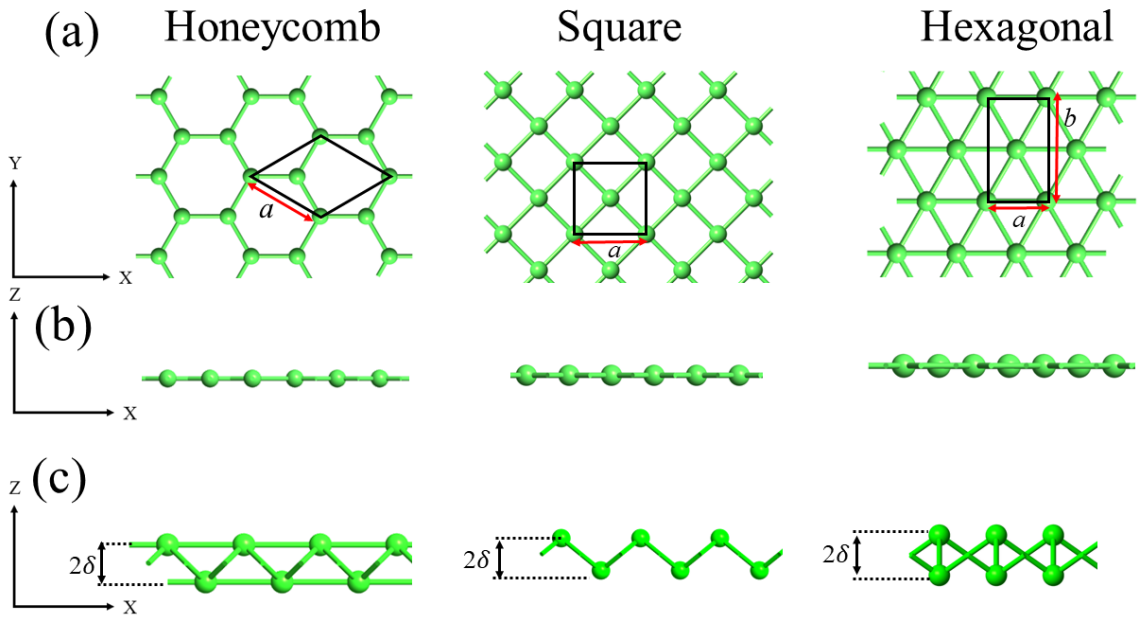

Figure 1: Schematics of 2D systems. The solid black line shows a computational unit cell. (a) Top view of planar and buckled systems. (b) Side view of planar systems. (c) Side view of buckled systems.

where $E_{N_k \times N_k \times 1}$ is the total energy at any given k-point N_k, and $E_{30\times30\times1}$ is the total energy at $N_k = 30$. The convergence tolerance of lower than 10 meV was achieved at $N_k = 13$ for all the studied systems (Figure 2a).

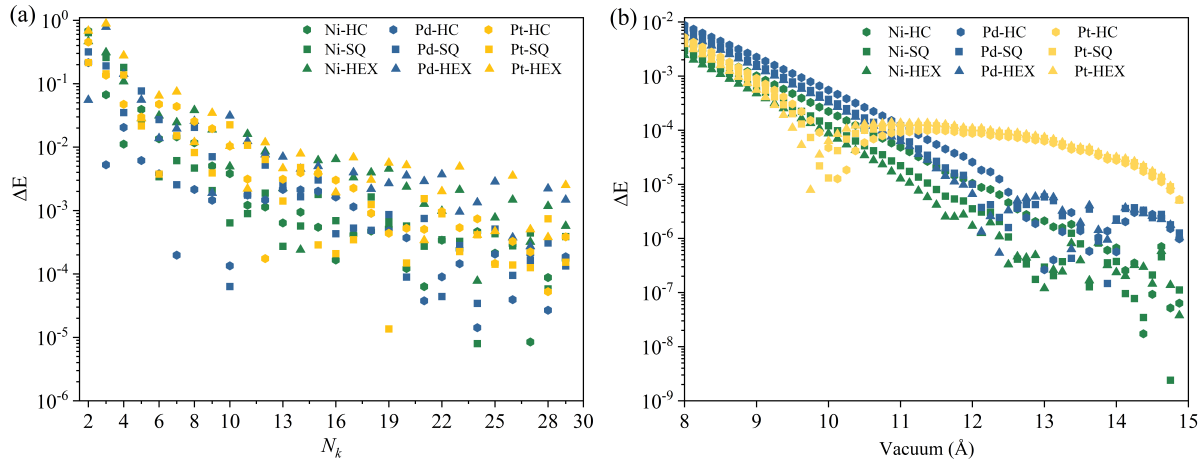

Figure 2: Convergence test plot on a logarithmic scale for 2D metals of group 10 (a) k-point (b) Vacuum.

3.1.2. Convergence test for vacuum: Using the converged k-point we will now perform the vacuum convergence analysis. Following the similar formalism as defined in Eq.(2). Now the

energy difference will be:

$$\Delta E = E_{vacuum} - E_{15Å}\,, \tag{2}$$

where E_{vacuum} is the total energy of the system at any given value of vacuum along the non-periodic direction of the 2D system, and $E_{15Å}$ is the total energy of the system having vacuum of 15 Å. The scattering in raw data becomes relatively small as compared to k-point convergence testing. Irrespective of the lattice type the data points obtained from a particular element were firmly stitched together (Figure 2b). However, for each element, the upper bound of the scattering envelope was of a honeycomb (HC) lattice, and the lower bound is of a hexagonal (HEX) lattice. Thus, the hexagonal lattice will converge relatively at a smaller vacuum compared to the honeycomb lattice. The square (SQ) lattice was embedded between HC and HEX for each element. With convergence criteria of less than 0.1 meV a vacuum of 13 Å was achieved for further calculations. However, for Pt, the set convergence criteria was satisfied around 10 Å but with a profound scattering. This can be attributed to non-monotonicity in energy differences and the sign change of ΔE results in an apparent dip when viewed on a logarithmic scale that considers only absolute values. In the subsequent calculations of geometric, energetic, and mechanical properties, we will use the obtained converged k-point and vacuum. However, before we get started with these analyses, it is necessary to provide an overview of the buckling mechanism and the method by which buckling parameters are selected in this article.

3.2. Buckling parameter:

The buckling is a phenomenon that enhances the overlapping of orbitals and by virtue of which a flat monolayer becomes buckled, i.e. the thickness of a planar 2D system towards the out-of-plane direction (Figure 1c). The extent of buckling is quantified by the value of parameter δ that quantifies the thickness of the system. Cartesian coordinates of two atoms placed in a computational unit cell will be different for a planar and buckled system in each symmetry (Table 1). For the initial guess of the buckling parameter δ, we considered the planar 2D systems and

Table 1: Atomic position in terms of bond length (d) in a unit cell of two atoms.

Systems	**Cartesian coordinates**	
	Atom-1	**Atom-2**
Honeycomb (HC)	d(0, 0, 0)	$d(1/\sqrt{3}, 2/\sqrt{3}, 0)$
Square (SQ)	d(0, 0, 0)	$d(1/\sqrt{2}, 1/\sqrt{2}, 0)$
Hexagonal (HEX)	d(0, 0, 0)	$d(1/2, \sqrt{3}/2, 0)$
Buckled honeycomb (BHC)	d(0, 0, δ)	$d(1/\sqrt{3}, 2/\sqrt{3}, -\delta)$
Buckled square (BSQ)	d(0, 0, δ)	$d(1/\sqrt{2}, 1/\sqrt{2}, -\delta)$
Buckled hexagonal (BHEX)	d(0, 0, δ)	$d(1/2, \sqrt{3}/2, -\delta)$

calculated the total energy variation with respect to the value of δ (Figure 3a). The potential energy surface (PES) of each system possesses a cusp demonstrating that the buckled systems are energetically more stable. Around this cusp, we use the equation of state $E = C + B\delta + A\delta^2$, where E is the total energy, A, B, and C are fitting parameters. Forces vanishes off at the minimum energy point i.e.: $F_\delta = \partial E/\partial\delta = 0$.

Using this logical approach the initial guess of the buckling parameters $\delta_{initial}$ were obtained for each buckled system. Upon relaxing the geometry, the optimized buckling parameter $\delta_{optimized}$ is obtained, and for each system, it was found that $\delta_{optimized} > \delta_{initial}$. The optimized δ for Pt is distributed around $0.1d_{3D}$ (d_{3D} is the bond length of 3D bulk) for each buckled structure (Table 2). However, for Ni and Pd the buckled honeycomb and square have the values of $\delta_{optimized}$ in the range $0.30d_{3D} - 0.45d_{3D}$, and for hexagonal, the $\delta_{optimized}$ is around

Table 2: Optimized geometrical dimensions ($a_{optimized}$ & $b_{optimized}$) of simulation box and corresponding optimized buckled parameter ($\delta_{optimized}$) in Å.

	Buckled honeycomb		**Buckled square**		**Buckled hexagonal**		
	$a_{optimized}$	$\delta_{optimized}$	$a_{optimized}$	$\delta_{optimized}$	$a_{optimized}$	$b_{optimized}$	$\delta_{optimized}$
Ni	2.413	1.0252	2.402	0.8680	2.418	3.58	0.4243
Pd	2.694	1.1727	2.652	1.0242	2.658	4.12	0.4468
Pt	4.084	0.3385	3.407	0.3882	2.642	4.30	0.2976

$0.15d_{3D}$. The buckled hexagonal of each element showed the lowest buckling effect. It was also revealed that for Ni and Pd the buckling effect decreases with an increase in coordination number. However, for the Pt, the buckling effect was largest for square followed by honeycomb and hexagonal systems (Table 2). The low-buckled structures have large simulation cells and the high-buckled structures have smaller simulation cells.

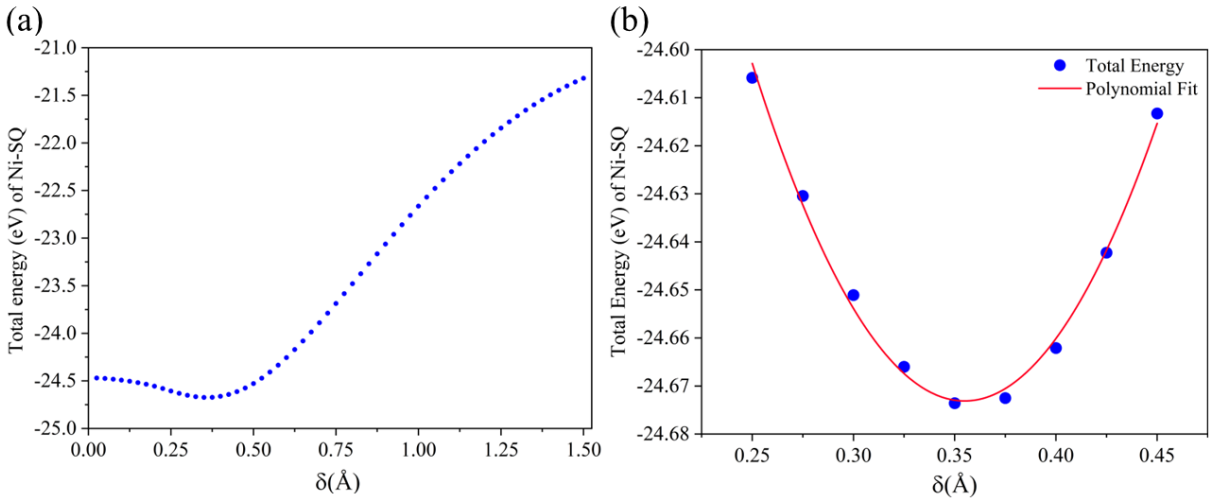

Figure 3: (a) Variation of total energy with respect to δ (b) Focused visualization around the cusp in PES

3.3. Bond length:

After examining the buckling for different lattices of group 10 elements, now we will discuss the calculated bond lengths of the optimized structures (Table 3). Bond lengths of 2D planar geometries of each element were in the agreement with previously reported results [6]. In 3D bulk, bond length increases as we move down a group, but in low dimensions, this trend is reversed for Pd and Pt. The geometric analysis revealed that the hexagonal buckled structures have shorter bonds than the planar monolayer for each element. Although the buckled structures in honeycomb and square form have larger bonds compared to flat monolayers. For Ni and Pd the longest bonds were in the BHC structure and the shortest bonds in HC. But the Pt showed the longest bond in HEX and the shortest in HC. The simulation box size and intra-layer atomic distance (d_{intra}) of buckled systems is found to be equal for each element (Table 2 & 3).

Table 3: Bond length (Å) of planar and buckled configurations. Intra-planar bond length denoted by d_{intra} and inter-planar bond length by d_{inter} .

	Honeycomb			**Square**			**Hexagonal**		
	HC	**BHC**		**SQ**	**BSQ**		**HEX**	**BHEX**	
	d	d_{intra}	d_{inter}	d	d_{intra}	d_{inter}	d	d_{intra}	d_{inter}
Ni	2.187	2.413	2.479	2.267	2.402	2.429	2.355	2.418	2.321
Pd	2.476	2.694	2.813	2.540	2.652	2.778	2.630	2.658	2.610
Pt	2.435	4.084	2.453	2.521	3.407	2.531	2.606	2.642	2.590

3.4. Cohesive Energies:
To investigate how the atomic cohesion is different for planar and buckled systems of group 10 elements we calculated the cohesive energy:

$$E_{coh} = E_{atom} - E_{system}/N\,, \tag{3}$$

where E_{atom} is the total energy of a single atom placed in a cube of length 15 Å, E_{system} is the total energy of the system and N is the number of atoms in the system. The calculated cohesive energies of each system were normalized to the 3D bulk cohesive energy [25] $E_{norm} = E_{coh}/E_{3D}$ and we considered it as a yardstick for each lattice and reflects the correlation of each system with the 3D bulk (Table 4). The general observations from the calculated cohesive energies are as follows. In planar 2D systems, each element in HC is the least stable and in HEX the most stable. For buckled systems, this trend is retained by Pt only and gets reversed for Ni and Pd. For all elements, the buckled system was found to be more stable than planar in each lattice. For Ni and Pd the high-buckled structure has higher cohesive energy than the low-buckled structure. This trend is not followed by Pt and BHEX has the highest cohesive energy although the highest buckling was observed in a square lattice. In general, the buckled systems showing high buckling have larger values of normalized cohesive energies (E_{norm}), which is an indication of their energetic correlation with 3D bulk.

Table 4: Cohesive Energies (E in eV) and normalized cohesive energies $E_{norm} = E_{coh}/E_{3D}$.

	Honeycomb				**Square**				**Hexagonal**			
	HC		**BHC**		**SQ**		**BSQ**		**HEX**		**BHEX**	
	E	E_{norm}	E	E_{norm}	E	E_{norm}	E	E_{norm}	E	E_{norm}	E	E_{norm}
Ni	2.837	0.64	4.163	0.94	3.240	0.73	3.950	0.89	3.610	0.81	3.680	0.83
Pd	1.974	0.51	3.200	0.82	2.362	0.61	3.025	0.78	2.656	0.68	2.773	0.71
Pt	3.751	0.64	3.831	0.65	4.115	0.70	4.383	0.75	4.620	0.79	4.701	0.80

3.5. Elastic Constants and Moduli:
Having observed the effect of buckling on geometric and energetic properties we will now focus on the elastic properties of the planar and buckled 2D systems of group 10 metals. For this purpose, the second-order elastic constants were determined within the linear elastic region. In 2D systems, the strain tensor is defined as:

$$\epsilon^{2D} = \begin{pmatrix} \varepsilon_1 & \varepsilon_6/2 \\ \varepsilon_6/2 & \varepsilon_2 \end{pmatrix}. \tag{4}$$

The elastic strain energy per unit area is given by $\Delta U(\varepsilon_i) = U(\varepsilon_i) - U(0)$, where $U(\varepsilon_i)$ represents energy density of strained system and $U(0)$ is the energy density of unstrained system.

$$\Delta U(\varepsilon_i) = \frac{1}{2}(C_{11}\varepsilon_1^2 + C_{22}\varepsilon_2^2 + 2C_{12}\varepsilon_1\varepsilon_2 + 2C_{16}\varepsilon_1\varepsilon_6 + 2C_{26}\varepsilon_2\varepsilon_6 + C_{66}\varepsilon_6^2)\,. \tag{5}$$

The C'^s_{ij} are the elastic constants and computed by taking the second-partial derivative of energy density with respect to strain in different directions $\partial^2\Delta U/\partial\varepsilon_i\varepsilon_j$. The elastic constants were calculated by using the formalism given in Refs. [26, 27] for different 2D crystal systems. While evaluating the elastic constants it was taken into consideration that the rectangular computational unit cell was used to simulate the 2D Hexagonal lattice (Figure 1a). For a rectangular computational cell all four elastic constants C_{11}, C_{12}, C_{22}, and C_{66} are independent. For square unit cells only three elastic constants C_{11}, C_{12}, and C_{66} are independent. For hexagonal unit cells only C_{11} and C_{12} are independent elastic constants and $C_{66} = (C_{11} - C_{12})/2$. The elastic moduli and Poisson's ratio were evaluated using the C'^s_{ij} in formulae [28] Young's modulus $\mathrm{Y} = (C_{11}^2 - C_{12}^2)/C_{11}$, Bulk modulus $\mathrm{B} = (C_{11} + C_{12})/2$, Shear modulus $\mathrm{G} = C_{66}$, and Poisson's ratio $\mu = C_{12}/C_{11}$.

For elastic stability, the elastic constants should always be positive and $C_{11} > C_{12}$ [27, 28]. Following this elasticity criterion, we found that the square lattices whether it is planar or buckled are structurally unstable (Table 5). The bulk moduli of 2D planar structures correlate with experimental bulk modulus as previously reported [6, 25]. Buckled structures have larger bulk moduli than planar bulk moduli with an exception of buckled hexagonal of Pd. It was observed that systems possessing a higher buckling effect have high values of bulk moduli. The highest change in bulk modulus was observed when the planar HC of Pd changes to BHC.

Table 5: Elastic constants, Young's modulus (Y), Bulk modulus (B), Shear modulus (G), and Poisson's ratio for each configuration. (Elastic constants and moduli are in units of GPa-nm and the Poisson's ratio has no unit.)

		$\mathbf{C_{11}}$	$\mathbf{C_{12}}$	$\mathbf{C_{22}}$	$\mathbf{C_{66}}$	**Y**	**B**	**G**	μ
Ni	**HC**	53.91	29.06	53.91	12.42	38.24	41.49	12.42	0.54
	BHC	190.58	66.84	190.58	61.87	167.14	128.71	61.87	0.35
	SQ	33.76	81.06	33.76	44.41	−160.88	57.41	44.40	2.40
	BSQ	146.43	23.56	146.43	−2.13	142.65	84.99	−2.13	0.16
	HEX	102.74	41.89	101.98	40.06	85.54	72.32	40.06	0.41
	BHEX	102.27	42.85	79.53	35.88	79.18	72.56	35.88	0.42
Pd	**HC**	47.44	21.70	47.44	12.87	37.51	34.57	12.87	0.45
	BHC	161.35	66.08	161.35	47.63	134.28	113.72	47.63	0.41
	SQ	53.35	54.25	53.35	29.14	−1.81	53.80	29.14	1.01
	BSQ	85.61	97.10	85.61	53.08	−24.51	91.35	53.08	1.13
	HEX	166.50	63.75	165.84	66.03	141.99	115.13	66.03	0.38
	BHEX	95.36	45.15	81.35	35.89	70.30	70.26	35.89	0.47
Pt	**HC**	77.08	38.66	77.08	19.21	57.69	57.87	19.21	0.50
	BHC	84.89	36.91	84.90	23.99	68.85	60.90	23.99	0.43
	SQ	87.14	93.67	87.14	26.70	−13.54	90.40	26.70	1.07
	BSQ	85.61	97.10	85.61	53.09	−24.51	91.35	53.08	1.13
	HEX	166.50	63.76	165.84	66.04	142.00	115.13	66.03	0.38
	BHEX	160.24	70.85	153.39	63.67	127.52	115.54	63.67	0.44

3.6. Projected Density of States (PDOS):

From the analysis of geometric, energetic, and mechanical properties it was revealed that 2D planar structures start to behave quite differently upon buckling. To understand this distinct behaviour we will now investigate the electronic structure of the different 2D lattices and will compare them with 3D bulk. In the ground state, the valence electrons of group 10 elements are accommodated in s and d orbitals. Thus, to realize the electronic structure of the Ni, Pd, and Pt it is reasonable to get to know the contribution of these orbitals to the total density of states. However, we also included the contribution from p orbitals in our analyses for the sake of completeness. The optimized structures obtained were selected and orbital-projected electron density of states (DOS) was evaluated using the k-point mesh of $13 \times 13 \times 1$. We used the Gaussian spectrum method with a smearing of 0.3 eV. From the DOS analysis, it was unveiled that the d states dominate the density of states for group 10 elements in 2D as well as in 3D bulk below Fermi-level. The d states are scarce above the Fermi level. The 2D planar honeycomb lattice has the highest number of available s states below the Fermi level when compared to other 2D systems. The $4d$ element which is Pd has the p states distributed around the Fermi-level for each 2D system. However, the $5d$ element which is Pt has strong peaks around the Fermi-level for planar honeycomb, otherwise all other 2D systems have distributed p states similar to $4d$ element. The p states of 2D systems of Ni are also distributed around the Fermi-level, but the p states in 3D bulk are unavailable around the Fermi-level. In general, it was observed that in the buckled systems in which the buckling effect is high the electrons in s, p, and d states resemble more closely to 3D bulk than 2D monolayer's PDOS.

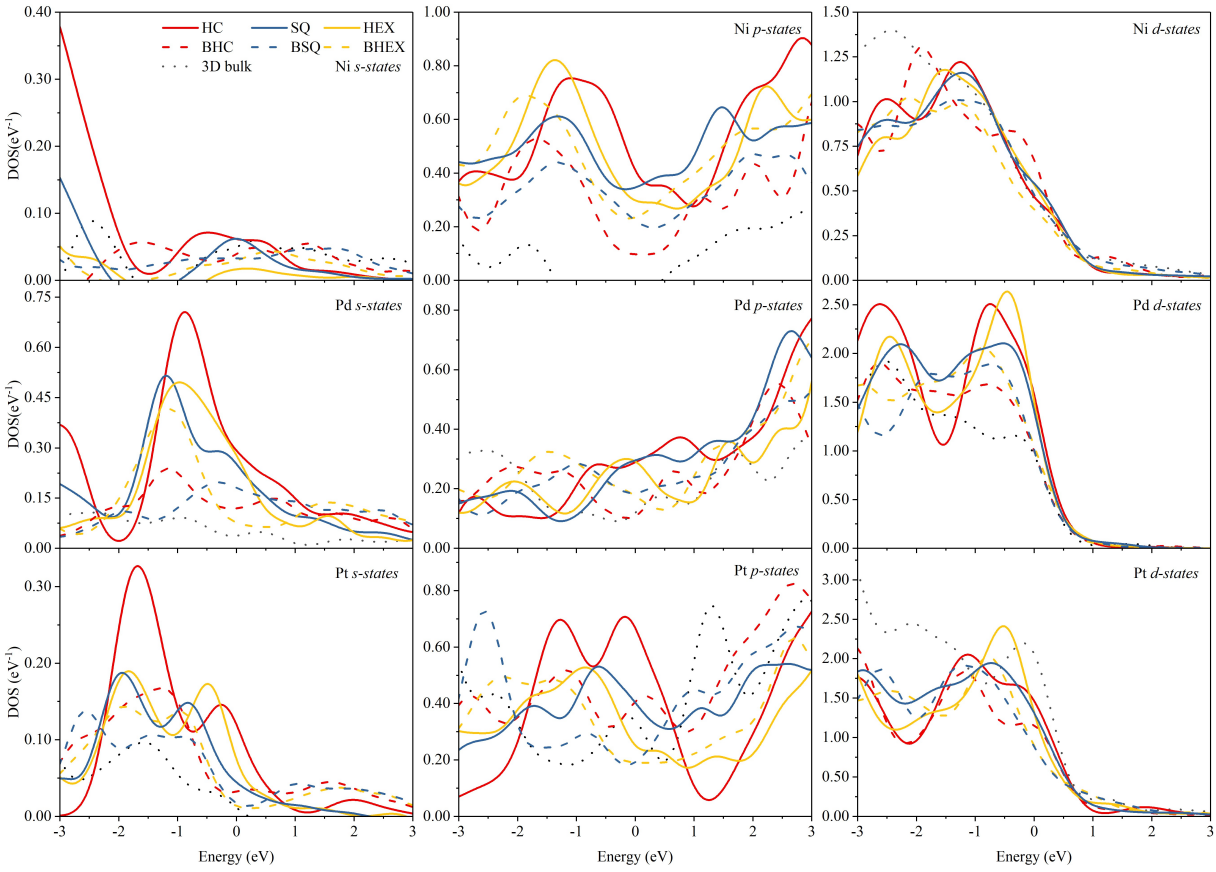

Figure 4: DOS projected on s, p, and d orbitals of 2D systems of group 10 elements in the planar and buckled form. 3D bulk is added for comparison.

4. Conclusion

We systematically studied the planar and buckled 2D systems of group 10 elements. We found that the ground state of 2D buckled systems of Pt possesses low buckling compared to Ni and Pd. The low buckling in Pt means planar preference and it can be related to the relativistic effects. The highest buckling effect was identified in Pd-BHC and the lowest in Pt-BHEX. In buckled structures, the highest cohesion was in the honeycomb structure for Ni and Pd, but in the hexagonal for Pt. The cohesive energy increases monotonically from honeycomb to hexagonal for Pt in planar as well as in buckled form. The in-plane elastic constants indicate that all elements of group 10 are unstable in a square lattice whether it is planar or buckled. There is an indication that the buckling effect correlates with bulk modulus as the buckling enhances the bulk modulus except for Pd-BHEX. In general, the electronic structure calculations revealed that in the structures in which the extent of buckling is high their PDOS can be better approximated by 3D bulk rather than the 2D planar monolayer. In summary, the geometric, energetic, elasticity, and DOS analyses are a reasonable starting point for understanding the different behaviour of planar and buckled structures. But still, understanding the inherent driving force which dictates the extent of buckling requires additional analyses which may give better insight. Although Ni, Pd, and Pt belong to the same group of the periodic table, their physical properties differ greatly in planar and buckled forms, so a theoretical study incorporating local and non-local correlations, relativistic effects, and spin-orbit coupling (SOC), is especially desirable.

References

[1] Zhao J *et al.* 2014 *Science* **343** 1228–1232
[2] Yang L M, Dornfeld M, Frauenheim T and Ganz E 2015 *Phys. Chem. Chem. Phys.* **17** 26036–26042
[3] Yang L M, Frauenheim T and Ganz E 2015 *Phys. Chem. Chem. Phys.* **17** 19695–19699
[4] Yang L M, Frauenheim T and Ganz E 2016 *Journal of Nanomaterials* **2016** 8429510
[5] Hoang V V *et al.* 2017 *Computational Materials Science* **126** 446–452
[6] Nevalaita J and Koskinen P 2018 *Phys. Rev. B* **97** 035411
[7] Nevalaita J and Koskinen P 2019 *Nanoscale* **11** 22019–22024
[8] Nevalaita J and Koskinen P 2020 *AIP Advances* **10** 065327
[9] Ono S 2020 *Phys. Rev. B* **102** 165424
[10] Ren Y, Hu L, Shao Y, Hu Y, Huang L and Shi X 2021 *J. Mater. Chem. C* **9** 4554–4561
[11] Ono S and Satomi H 2021 *Phys. Rev. B* **103** L121403
[12] Ono S 2021 *Phys. Rev. Materials* **5** 104004
[13] Ma Y, Li B and Yang S 2018 *Mater. Chem. Front.* **2** 456–467
[14] Chen Y, Fan Z, Zhang Z, Niu W, Li C, Yang N, Chen B and Zhang H 2018 *Chemical Reviews* **118** 6409–6455
[15] Wang T, Park M, Yu Q, Zhang J and Yang Y 2020 *Materials Today Advances* **8** 100092
[16] Ta Huy Q *et al.* 2021 *Advanced Science* **8** 2100619
[17] Mujib S B, Ren Z, Mukherjee S, Soares D M and Singh G 2020 *Materials Advances* **1** 2562–2591
[18] Fan F R, Wang R, Zhang H and Wu W 2021 *Chemical Society Reviews* **50** 10983–11031
[19] Smidstrup S *et al.* 2019 *Journal of Physics: Condensed Matter* **32** 015901
[20] Bløchl P E 1994 *Phys. Rev. B* **50** 17953–17979
[21] Kresse G and Furthmüller J 1996 *Phys. Rev. B* **54** 11169–11186
[22] Perdew J P, Burke K and Ernzerhof M 1996 *Phys. Rev. Lett.* **77** 3865–3868
[23] Liu D C and Nocedal J 1989 *Mathematical Programming* **45** 503–528
[24] Monkhorst H J and Pack J D 1976 *Phys. Rev. B* **13** 5188–5192
[25] Kittel C and McEuen P 2018 *Introduction to solid state physics* (John Wiley & Sons) p 50
[26] Wang V, Xu N, Liu J C, Tang G and Geng W T 2021 *Computer Physics Communications* **267** 108033
[27] Maździarz M 2019 *2D Materials* **6** 048001
[28] Zhang S and Zhang R 2017 *Computer Physics Communications* **220** 403–416